Cluster-Supercluster Alignments

Jounghun Lee[1] and August E. Evrard[2,3,4]

ABSTRACT

We study correlations in spatial orientation between galaxy clusters and their host superclusters using a Hubble Volume N-body realization of a concordance cosmology and an analytic model for tidally-induced alignments. We derive an analytic form for distributions of the alignment angle as functions of halo mass (M), ellipticity (ϵ), distance (r) and velocity (v) and show that the model, after tuning of three parameters, provides a good fit to the numerical results. The parameters indicate a high degree of alignment along anisotropic, collapsed filaments. The degree of alignment increases with M and ϵ while it decreases with r and is independent of v. We note the possibility of using the cluster-supercluster alignment effect as a cosmological probe to constrain the slope of the initial power spectrum.

Subject headings: cosmology:theory — large-scale structure of universe

1. INTRODUCTION

Superclusters are collections of galaxy groups and clusters that represent the largest, gravitationally bound structures in the universe (Shapley 1930; Kalinkov et al. 1998). If the dark energy is a cosmological constant, then the collapse of these systems over the next few billion years of the cosmic future will mark the end of hierarchical structure formation in our universe (Nagamine & Loeb 2003; Busha et al. 2005). A conspicuous feature of locally observed superclusters is the strong tendency of member clusters to be elongated in their

[1]Department of Physics and Astronomy, FPRD, Seoul National University, Seoul 151-747 , Korea

[2]Department of Astronomy and Michigan Center for Theoretical Physics, University of Michigan, Ann Arbor, 500 Church St., MI 48109, USA

[3]Department of Physics and Michigan Center for Theoretical Physics, University of Michigan, Ann Arbor, 450 Church St.,MI 48109-1040, USA

[4]Visiting Miller Professor, Physics Department, University of California, Berkeley, CA94720, USA

major axis orientations (Plionis 2002, 2004), which is in turn closely related to their filamentary shapes (e.g., Basilakos 2003). To describe the structure distribution on the largest scale in the universe, it will be quite essential to understand this effect of cluster-supercluster alignments from first principles.

The effect of structure-substructure alignment is in fact observed on all different scales in the universe. On the subgalactic scale the galaxy satellites are observed to be located preferentially near the major axes of their host galaxies (Valtonen et al. 1978; Knebe et al. 2004; Brainerd 2005; Agustsson & Brainerd 2006). On the galactic scale the major axes of cluster galaxies are observed to be aligned with that of their host clusters (Plionis & Basilakos 2002; Plionis et al. 2003). The cluster galaxies are also observed to have a strong tendency toward radial alignment (Pereira & Kuhn 2005).

Although this alignment effect has been shown to be a natural outcome in the currently favored concordance ΛCDM cosmology (Onuora & Thomas 2000; Libeskind et al. 2005; Kang et al. 2005; Lee et al. 2005; Zentner et al. 2005; Kasun & Evrard 2005; Basilakos et al. 2006), its detailed origin remains a subject of debate between those who emphasize the importance of anisotropic merging and those who stress tidal interaction.

The anisotropic merging scenario explains that the effect of substructure-structure alignment is induced by the anisotropic merging and infall of matter along filaments (West 1989). It was indeed shown by N-body simulations that the merging and infall of matter to form bound halos indeed occur preferentially along filaments, which provided supporting evidences for this scenario (e.g., West 1991; van Haarlem & van de Weygaert 1993; Dubinski 1998; Faltenbacher et al. 2002; Knebe et al. 2004; Zentner et al. 2005).

The tidal interaction theory explains that the correlations between the substructure angular momentum vectors and the principal axes of the host tidal fields induce the alignment effect. Lee et al. (2005) constructed an analytic model for the effect of substructure alignment in the frame of the tidal interaction theory, and showed that their analytic predictions are in good agreement with the numerical results from N-body simulations.

In fact, the above two theories are not mutually exclusive since the anisotropic merging and infall itself is a manifestation of the primordial tidal field (Bond, Kofman, & Pogosyan 1996). The difference between the two scenarios, however, lies in the question of whether the connection to filaments is a major contribution or not.

Very recently, Atlay et al. (2006) have quantified the influences of both the tidal interaction and the anisotropic infall through the analysis of data from recent high-resolution N-body simulations. What they confirmed is the following: (i) For the majority of halos the alignment effect is caused by the tidal field but not by the anisotropic infall; (ii) Only for

the cluster-size halos the alignment effect is dominantly due to the anisotropic merging and infall of matter along filaments. In other words, they made it clear that the filaments are important marker of local orientations on the cluster halo scale.

Now that the cluster-supercluster alignment turns out to be due to the anisotropic merging along filaments, it is desirable to have a theoretical frame work within which one can provide physical answers to the remaining questions such as how the alignment effect depends on the cluster properties such as mass, shape, and etc. Our goal here is to construct such a theoretical framework by using both analytical and numerical methods. Analytically we adopt the standard cosmic web theory, and numerically we use the large Hubble volume simulation data.

The organization of this paper is as follows. In §2 we provide a brief description of the Hubble volume simulation and summarize the numerical results. In §3 we present an analytic model and compare its predictions with the numerical results. In §4 we discuss our results and draw final conclusions.

2. NUMERICAL RESULTS

For the numerical analysis, we use a mass-limited sample of cluster halos extracted from the Hubble Volume simulation of a ΛCDM universe (Evrard et al. 2002). The simulation models dark matter structure resolved by particles of mass $m = 2.25 \times 10^{12} h^{-1} M_{\odot}$ in a periodic cube of linear size $3000 h^{-1}$Mpc, assuming $\Omega_m = 0.3, \Omega_\Lambda = 0.7$ and $\sigma_8 = 0.9$. The $z = 0$ catalog contains a total of 82973 halos with mass above a limiting value $M > 3 \times 10^{14} h^{-1} M_{\odot}$, with information on various properties such as center-of-mass position, mass, inertia momentum tensor, and redshift. We refer the readers to Evrard et al. (2002) and Kasun & Evrard (2005) for the details of the cluster catalog, including the algorithm of cluster identification.

The superclusters are identified in the catalog with the help of the friends-of-friends algorithm with the linking length of $0.33\bar{l}$, where $\bar{l} = 69 h^{-1}$Mpc is the mean spacing of the mass-limited sample. The total number and the mean mass of the identified superclusters are $N_s = 14007$ and $\bar{M}_s = 1.26 \times 10^{15} h^{-1} M_{\odot}$, respectively. This large number of superclusters allows us to study the alignment effect with high statistical power.

Figure 1 shows orthogonal projections of the third richest supercluster in the volume. It contains 12 halos above the applied mass limit, and a total mass of $5.3 \times 10^{15} h^{-1}\,\mathrm{M}_{\odot}$ associated with these halos. The spatial distribution of the supercluster is highly elongated, much closer to filamentary than spherical. In this example, the major axis orientations of the

halos, taken from Kasun & Evrard (2005), are shown as whiskers in the plot. The tendency for these halos to be aligned with their supercluster's principal axis, although arguably visible in this plot, is a weak effect. We therefore seek a statistical measure using the entire supercluster sample.

For each supercluster, we measure its inertia momentum tensor, $\mathbf{I}^s \equiv (I^s_{ij})$, as

$$I^s_{ij} = \frac{1}{M_s} \sum_{\alpha} M^{\alpha}_c x^{\alpha}_{c,i} x^{\alpha}_{c,j}, \tag{1}$$

where M^{α}_c and $\mathbf{x}^{\alpha}_c \equiv (x^{\alpha}_{c,i})$ represent the mass and the position of the α-th member cluster, respectively and M_s is the total mass of the host supercluster. Then, we compute the eigenvalues and eigenvectors through the diagonalization of $\mathbf{I}^s$ and determine the major-axis direction as the direction of the eigenvector corresponding to the largest eigenvalue.

It is, however, worth mentioning here that for a supercluster which has less than five clusters, the orientation of its major axis derived using equation (1) must suffer from considerable inaccuracy. The most idealistic way should be to derive the major axis of a supercluster using all particles within it.

Nevertheless, given that the major axes of the superclusters in real observations cannot be determined by this idealistic way since the positions of the dark matter particles are not measurable, the advantage of our analysis based (eq.[1]) is its practicality. That is, it can be readily repeated by observers based directly on cluster catalogs.

At any rate, to overcome the limitation of our analysis based on equation (1, we construct a separate sample choosing only those superclusters which have more than five clusters ($N_c > 5$ where N_c is the number of clusters within the superclusters). It is found that 217 superclusters have more than five clusters and total 1492 clusters belong to those 217 superclusters.

First, we measure the probability distribution of the cosines of the angles, $\cos\theta$, between the major axes of the superclusters and their member clusters. Figure 2 plots the result as solid dots with Poisson errors. The upper panel corresponds to the case that all the $14,007$ superclusters are used, while the lower panel corresponds to the case that only those superclusters with more than five clusters are used. The dotted line in each panel corresponds to the case of no alignment. As can be seen, the distribution, $p(\cos\theta)$, increases with $\cos\theta$ in the both panels, revealing a clear signal of alignment effect. Although the result of the lower panel shows less sharp increase, suffering from large errors, the signal is robust at the 99% confidence level. It indicates that the cluster-supercluster alignment effect is not a false signal originated from the inaccurate derivation of the supercluster major axes but a real one. The mean value of $\cos\theta$ is found to be 0.54 and 0.52 in the upper and the lower panels,

respectively.

Now that a robust signal of cluster-supercluster alignment effect is found, we examine how the degree of the alignment depends on the cluster properties. First, we examine how the average of $\cos\theta$ depends on the cluster mass, M_c. Figure 3 plots the result versus the rescaled cluster mass, $\tilde{M} \equiv M_c/M_s$, as solid dots with errors which are calculated as one standard deviation of $\cos\theta$ for the case of no alignment. As can be seen in the upper panel, the degree of alignment increases with $\tilde{M}$. A similar trend is also shown in the lower panel although it suffers from the large errors.

Second, we examine how the average of $\cos\theta$ depends on the separation distance, r, from the supercluster center to the cluster center. Figure 4 plots the result versus the rescaled distance, $\tilde{r} \equiv r/R_s$ as solid dots with errors. As can be seen in the upper panel, the degree of the alignment decreases with distance. That is, the closer a cluster is located to the supercluster center,the more stronger the alignment effect is.

Third, we examine how the average of $\cos\theta$ depends on the cluster ellipticity, ϵ. Here, we define the ellipticity of a cluster as $\epsilon \equiv 1 - \sqrt{\varrho_3^c/\varrho_1^c}$ assuming a prolate cluster shape, where ϱ_1^c and ϱ_3^c are the largest and the smallest eigenvalues of the cluster inertia momentum tensor, respectively. Figure 5 plots the result versus the rescaled ellipticity, $\tilde{\epsilon} \equiv \epsilon/\epsilon_0$ (where ϵ_0 is the maximum cluster ellipticity) as solid dots with errors, which reveals that the degree of alignment increases with cluster ellipticity. That is, the more elongated a cluster is, the more stronger the alignment effect is.

Fourth, we measure the average of $\cos\theta$ as a function of the cluster velocity, v. Figure 6 plots the result with solid dots with errors, which reveals that the degree of alignment depends very weakly on the cluster velocity.

We provide physical explanations for these numerical results in §3.

3. PHYSICAL ANALYSIS

3.1. *Hypotheses*

To construct an analytic model for the cluster-supercluster alignment effect, we assume the following.

1. A supercluster forms through anisotropic merging of clusters along filaments. In consequence, the major axis of a supercluster tends to be in the direction of the dominant filament. A filament is defined as one dimensional object collapsed along the major and

intermediate principal axes of the local tidal tensor (Zeldovich 1970; Pogosyan et al. 1998). The direction of a filament thereby is aligned with the minor principal axis of the tidal tensor. Therefore, the major axis of a supercluster tends to be in the direction of the minor principal axis of the tidal tensor.

2. Let $\mathbf{T}^s$ be the tidal tensor field smoothed on the supercluster mass scale, and let also $\delta_s \equiv \Delta\rho/\bar{\rho}$ be the linear density contrast of the supercluster where $\bar{\rho}$ is the mean mass density. Let also $\lambda_1, \lambda_2, \lambda_3$ (with $\lambda_1 > \lambda_2 > \lambda_3$) be the three eigenvalues of $\mathbf{T}^s$. The collapse condition for a supercluster is given as

$$\delta_s = \lambda_1 + \lambda_2 + \lambda_3 = 1.3, \qquad \lambda_1 > \lambda_2 > 0, \quad \lambda_3 < 0. \tag{2}$$

Given that the supercluster passes the moment of turn-around but not yet virialized, we expect its linear density contrast, δ_s, to be in the range $(1, 1.68)$ where the values of 1 and 1.68 correspond to the linear densities at the moments of the turn-around and the virialization, respectively (Eke et al. 1996). Here, we choose a fiducial value of $\delta_s = 1.3$. The other condition, $\lambda_1 > \lambda_2 > 0, \lambda_3 < 0$ in equation (2) represents the collapse along filaments (Pogosyan et al. 1998).

3. The cluster-supercluster alignment is a reflection of the anisotropic spatial distribution of cluster galaxies in a filament-dominant web-like cosmic structure. The correlation of the spatial positions of galaxies with the local tidal field can be quantified by the following quadratic equation which was first suggested by Lee & Kang (2006).

$$\langle x_i^c x_j^c | \hat{\mathbf{T}}^s \rangle = \frac{1-s}{3}\delta_{ij} + s\hat{T}_{ik}^s \hat{T}_{kj}^s, \tag{3}$$

where $\mathbf{x}^c \equiv (x_i^c)$ and $\hat{\mathbf{T}}^s = (\hat{T}_{kj}^s) \equiv T_{ik}^s/|\mathbf{T}^s|$ are the rescaled major axis of a galaxy cluster and the unit tidal shear tensor smoothed on the supercluster mass scale, M_s. Here, the parameter, $s \in [-1, 1]$, represents the strength of the correlation between $\mathbf{x}^c$ and $\mathbf{T}^s$. If $s = -1$, there is the strongest correlation between $\mathbf{x}^c$ and $\hat{\mathbf{T}}^s$. If $s = 1$, there is the strongest anti-correlation between $\mathbf{x}^c$ and $\hat{\mathbf{T}}^s$. While if $s = 0$, there is no correlation between them.

4. The conditional probability distribution of $\mathbf{x}^c$ provided that the local tidal field is given as $\mathbf{T}^s$ can be approximated as Gaussian (Lee & Kang 2006):

$$P(\mathbf{x}^c|\hat{\mathbf{T}}^s) = \frac{1}{[(2\pi)^3 \det(M)]^{1/2}} \exp\left[-\frac{x_i^c (M^{-1})_{ij} x_j^c}{2}\right], \tag{4}$$

where the covariance matrix $M_{ij} \equiv \langle x_i^c x_j^c | \hat{\mathbf{T}}^s \rangle$ is related to $\hat{\mathbf{T}}^s$ by equation (3).

It is worth mentioning here the difference of the cluster-supercluster alignment from the galaxy-cluster alignment. For the former case, the primordial tidal field induces the anisotropy in the spatial distribution of galaxies along cosmic filaments, which results in the alignment between the major axes of clusters and their superclusters. For the latter case, the tidal field of a virialized cluster halo induces the angular momentum of the cluster galaxies whose minor axes tend to be aligned with the major axis of its host cluster (Lee et al. 2005). In other words, the alignments between the major axes of cluster galaxies and their host clusters are related to the generation of the angular momentum while the alignments between the major axes of clusters and their host superclusters related to the filamentary distribution of galaxies.

3.2. *Analytic Expressions*

Using the four hypotheses given in §3.1, we derive first $p(\cos\theta)$ analytically. According to the second hypothesis, it amounts to deriving the probability density distribution of the cosines of the angles between the major axes of clusters and the minor principal axes of the local tidal tensors.

Let us express $\mathbf{x}^c$ in terms of the spherical polar coordinates in the principal axis frame of $\mathbf{T}^s$ as $\mathbf{x}^c = (x^c \sin\theta\cos\phi, x^c \sin\theta\sin\phi, x^c\cos\theta)$ where $x^c \equiv |\mathbf{x}^c|$ and θ and ϕ are the polar and the azimuthal angles of $\mathbf{x}^c$, respectively. Then, the polar angle, θ, is nothing but the angle between $\mathbf{x}^c$ and the minor principal axis of $\mathbf{T}^s$. Now, the probability density distribution of $\cos\theta$ can be derived by integrating equation (4) over x^c and ϕ as $p(\cos\theta) = \int_0^{2\pi}\int_0^\infty P(x^c,\theta,\phi)x^{c2}dx^c d\phi$, which leads to (Lee & Kang 2006)

$$p(\cos\theta) = \frac{1}{2\pi}\prod_{i=1}^{3}\left(1-s+3s\hat{\lambda}_i^2\right)^{-\frac{1}{2}} \times \int_0^{2\pi}\left(\frac{\sin^2\theta\cos^2\phi}{1-s+3s\hat{\lambda}_1^2}+\frac{\sin^2\theta\sin^2\phi}{1-s+3s\hat{\lambda}_2^2}+\frac{\cos^2\theta}{1-s+3s\hat{\lambda}_3^2}\right)^{-\frac{3}{2}} d\phi, \quad (5)$$

where $\{\hat{\lambda}_i\}_{i=1}^3$ are the unit eigenvalues of $\hat{\mathbf{T}}$ related to $\{\lambda_i\}_{i=1}^3$ as $\hat{\lambda}_i \equiv \lambda_i/\left(\lambda_1^2+\lambda_2^2+\lambda_3^2\right)^{1/2}$.

It was in fact Lee & Kang (2006) who first derived equation (5) as an analytic expression for the probability distribution of the alignments between the positions of the galaxy satellites in the major axis orientations of their host galaxies. Here, we derive it as an analytic expression for the probability distribution of the alignments between the major axes of clusters and their host superclusters. It is important to note a key difference between the two cases. For the case of galaxy satellites, it is the tidal fields of the *virialized* galactic halos

that causes the alignment effect. Therefore, all the eigenvalues, $\lambda_1, \lambda_2, \lambda_3$ in equation (5) should be positive. Whereas for the case of clusters in superclusters it is the local filaments which collapse along only two principal axes of the primordial local tidal tensors. Therefore, λ_3 in equation (5) has a negative value.

The probability distribution, $p(\cos\theta)$ (eq.[5]) is characterized by three independent parameters, s, λ_1, and λ_2. Once the values of λ_1 and λ_2 are determined, then the negative value of λ_3 is automatically determined by equation (2). Since the values of these three parameters depend on the properties of individual superclusters as well as the local conditions of the initial tidal fields, it may be quite difficult to determine them analytically.

Instead, we determine their average values by fitting equation (5) to the numerical results obtained in §2. When the numerical result using all superclusters are fitted, the best-fit values of the three parameters are found to be $s = -0.71$, $\lambda_1 = 2.23$, and $\lambda_2 = 0.53$, which gives $\lambda_3 = -1.46$. When the numerical result using only those superclusters with $N_c > 5$ are fitted, it is found interestingly that the best-fit values of the parameters are $s = -0.5$, $\lambda_1 = 2.23$, and $\lambda_2 = 0.53$. Note that the two numerical cases yield the same best-fit values for λ_1 and λ_2 although the best-fit values of the correlation parameters are different as $s = -0.71$ and $s = -0.5$.

Figure 2 plots the analytic distributions with these best-fit parameters (solid line) and compares it with the numerical data points. In the upper panel, the analytic distribution with $s = -0.71$ is compared with the numerical result obtained in §2 using all superclusters, while in the lower panel the analytic distribution with $s = -0.5$ is compared with the numerical result obtained using only those superclusters with more than five clusters ($N_c > 5$). As can be seen, the analytic and the numerical results are in good agreement with each other in the both panels.

It is worth mentioning here that the best-fit values of the three parameters are subject to our fiducial choice of $\delta_s = 1.3$. As mentioned in §3.1, there is no consensus on the critical linear density of the superclusters unlike the case of clusters. Varying the value of δ_s from 1.0 to 1.68, we have repeated the fitting procedure, and we found that although the best-fit values of λ_1 and λ_2 change by maximum 20%, the fitting result itself does not sensitively change with the value of δ_s. Thus, it is concluded that our fiducial model is a stable choice.

Now that we have the probability density distribution, $p(\cos\theta)$, we would like to find an analytic expression for $\langle\cos\theta\rangle$ as a function of cluster mass, position, ellipticity, and velocity. The dependence of the correlation parameter s on the cluster mass M may be obtained by considering the difference in mass between the cluster and its host supercluster. Strictly speaking, equation (3) is valid when the tidal tensor $\mathbf{T}^s$ and the position vector

$\mathbf{x}^c$ are smoothed on the same mass scale. In other words, the correlation between $\mathbf{x}^c$ and $\mathbf{T}^s$ is expected to be highest when the two smoothing mass scales are the same. In reality, however, $\mathbf{T}^s$ is smoothed on the supercluster mass scale M_s while $\mathbf{x}^c$ is smoothed on the cluster mass scale M_c. The difference between the two mass scales diminishes the correlation between $\mathbf{x}^c$ and $\mathbf{T}^s$.

Let s_{M_0} be the value of the correlation parameter when the tidal field is smoothed on the same cluster mass scale, $\mathbf{T}^c$. We expect $s_{M_0} = -1$. Given equation (3), we approximate $s = s(\tilde{M})$ as

$$s(\tilde{M}) \approx s_{M_0} \frac{\langle \hat{T}^s_{ik} \hat{T}^s_{kj} \rangle}{\langle \hat{T}^c_{ik} \hat{T}^c_{kj} \rangle} \approx s_{M_0} \frac{\sigma_s^2}{\sigma_c^2}. \tag{6}$$

Here, σ_c and σ_s represent the rms linear density fluctuations smoothed on the mass scales of M_c and M_s, respectively. In deriving equation(6) we use the approximation of $\langle \hat{T}^c_{ik} \hat{T}^c_{kj} \rangle \approx \langle T^c_{ik} T^c_{kj} \rangle / |\mathbf{T}^c|^2$, which was proved to be valid by Lee & Pen (2001).

Now that the functional form of $s(\tilde{M})$ is found, the average of $\cos\theta$ as a function of $\tilde{M}$ can be calculated by equations (5) and (6) as

$$\langle \cos\theta \rangle (\tilde{M}) = \int_0^\infty \cos\theta p[\cos\theta; s(\tilde{M})] d\cos\theta. \tag{7}$$

Figure 3 plots equation (7) with $\lambda_1 = 2.23$ and $\lambda_2 = 0.53$ (solid line), and compares it with the numerical result (dots) obtained in §2. For the analytic distribution, the value of M_s is set to be the mean mass of the superclusters found in §2: $1.26 \times 10^{15} h^{-1} M_\odot$ (upper panel); $3.69 \times 10^{15} h^{-1} M_\odot$ (lower panel). As can be seen, in the upper panel the analytic and the numerical results agree with each other excellently. In the lower panel, although the numerical result suffers from large errors, the analytic prediction is still quite consistent with the numerical result.

The dependence of the correlation parameter, s, on the distance, r, between the centers of clusters and their host superclusters can be obtained in a similar way. The correlation between $\mathbf{x}^c$ and $\mathbf{T}^s$ in equation (3) becomes strongest when $r = 0$. In reality, however, r always deviates from zero, which will diminish the correlation strength.

Let s_{r0} be the value of the correlation parameter when $r = 0$, which is expected again to be $s_{r0} = -1$. With a similar approximation made for equation (6), we find the following formula for $s(r)$:

$$s(r) \approx \frac{1}{2} s_{r0} \left[1 + \frac{\langle \hat{T}^c_{ij}(\mathbf{x}+\mathbf{r}) \hat{T}^c_{ij}(\mathbf{x}) \rangle}{\langle \hat{T}^c_{ij}(\mathbf{x}) \hat{T}^c_{ij}(\mathbf{x}) \rangle} \right] \approx \frac{1}{2} s_{r0} \left[1 + \tilde{\xi}_c(r) \right], \tag{8}$$

where $\tilde{\xi}_c(r)$ represents the two point density correlation rescaled to satisfy $\tilde{\xi}_c(0) = 1$. Since the distance r is a Eulerian quantity unlike the mass M_s, we use the Eulerian filtering radius of $2h^{-1}$Mpc, the typical cluster size, to convolve the correlation function $\tilde{\xi}_c$. Here, the factor of $1/2$ comes from the average decreases of the correlation parameter due to the mass difference between the clusters and their host superclusters.

Now that the functional form $s(r)$ is found, the average of $\cos\theta$ as a function of r can be calculated through equations (5) and (8) as

$$\langle\cos\theta\rangle(r) = \int_0^\infty \cos\theta p[\cos\theta; s(r)]d\cos\theta. \tag{9}$$

Figure 4 plots equation (9) (solid line) as a function of the rescaled distance, $\tilde{r} \equiv r/R_s$, and compares it with the numerical result (dots) obtained in §2. For the analytic distribution, the value of R_s is set to be the mean Lagrangian radius of superclusters found in §2 using the relation of $R_s = [3\bar{M}_s/(4\pi\bar{\rho})]^{1/3}$. As can be seen, the analytic and the numerical results agree with each other quite well.

Regarding the dependence of s on the cluster ellipticity, ϵ, although it is predicted qualitatively in our theoretical model that the degree of the alignment increases with ellipticity, the quantitative functional form of $s(\epsilon)$ is quite difficult to determine analytically since the cluster ellipticity are sensitively vulnerable to modifications caused by nonlinear merging and infall process.

Instead of using analytic approach, numerical fitting is used to determine the functional form of $s(\epsilon)$. Let $s_{\epsilon 0}$ represents the value of s when the cluster ellipticity has the maximum value, $\epsilon 0$. It is expected again that $s_{\epsilon 0} = -1$. We find that the following formula gives a good fit to the numerical results

$$s(\tilde{\epsilon}) = s_{\epsilon 0}\tilde{\epsilon}^{1/2}. \tag{10}$$

Since ϵ_0 is defined as the maximum ellipticity, $s(\tilde{\epsilon})$ has the extreme value of -1 at $\tilde{\epsilon} = 1$. Note that the value of ϵ_0 is not fixed but sample-dependent. Here, the Millennium Run data we use yields $\epsilon_0 = 0.7$. But, a different sample could yield a different value of ϵ_0.

Now that the functional form of $s(\tilde{\epsilon})$ is found, the average of $\cos\theta$ as a function of $\tilde{\epsilon}$ can be calculated by equations (5) and (10) as

$$\langle\cos\theta\rangle(\tilde{\epsilon}) = \int_0^\infty \cos\theta p[\cos\theta; s(\tilde{\epsilon})]d\cos\theta. \tag{11}$$

The comparison between the analytic result (eq.[11]) and the numerical data points shows good consistency, as seen in Fig. 5.

Regarding the dependence of s on the cluster velocity v, no strong dependence is expected in our model since the primordial tidal field is uncorrelated with the velocity field (Bardeen et al. 1986). Therefore, we model it as an uniform distribution as $\langle \cos\theta \rangle(v) = \langle \cos\theta \rangle$. The average value, $\langle \cos\theta \rangle$ is found to be 0.54 when $s = -0.71$ (upper panel) while it is 0.52 when $s = -0.5$ (lower panel). As can be seen in Fig. 6, the analytic and the numerical results are consistent with each other.

4. DISCUSSION AND CONCLUSION

In the context of the standard cosmic web picture of large-scale structure, we have constructed a parametric model for the alignment of cluster-sized halos with their host superclusters. The underlying assumption is that cluster-supercluster alignment reflects the spatial distribution of matter as it is organized along filamentary structures by the primordial tidal field. The parameters of the analytic model represent the dominance of filaments and the spatial coherence of the initial tidal field.

We show that the analytic model provides a good fit to orientation data derived from mass-limited halo samples of a ΛCDM Hubble volume simulation. After fitting the three free parameters using the overall distribution of cluster-supercluster alignment angles, the model then simultaneously matches the behavior of the mean alignments as a function of relative mass, cluster position within the supercluster, and cluster ellipticity. No trend with cluster velocity is predicted or measured in the simulation.

It is worth discussing a couple of simplified assumptions on which our theoretical model is based. First,we have used the FOF algorithm to identify superclusters in the N-body simulation data. Unlike the case of virialized clusters, however, there is no established consensus on how to define superclusters. Different supercluster-identification algorithms could result in different multiplicity, mass, and shape of superclusters which would in turn affect our results.

Second, we have assumed that the filaments correspond to the Lagrangian regions where only the largest and the second largest eigenvalues of the local tidal tensor are positive. Although this definition of a filament is consistent with the picture of the Zel'dovich approximation, it is obviously an oversimplification of the reality. A more realistic definition and treatment of cosmic filaments will be necessary to refine the model.

Another issue that we would like to discuss here is the possibility of using the cluster-supercluster alignment effect as a cosmological probe. We have shown that the phenomena of cluster-supercluster alignments are closely related to the dominance of filaments, the web-

like distribution of galaxies on very large scales. The dominance of filaments is in turn related to the spatial correlations of the primordial tidal field, which depends sensitively on the slope of the initial power spectrum on the supercluster scale. Thus, by measuring the degree of cluster-supercluster alignment, it might be possible to constrain the slope of the initial power spectrum in a complementary way.

Finally, we conclude that our model for the cluster-supercluster alignments will provide a theoretical framework within which the distribution of cosmic structures on the largest scales can be physically understood and quantitatively described.

We are grateful to the anonymous referee who helped us improve the original manuscript. We are also grateful to the warm hospitality of Y.Suto and the University of Tokyo, where this work was initiated. J.L. also thanks D. Park for useful helps. J.L. is supported by the research grant No. R01-2005-000-10610-0 from the Basic Research Program of the Korea Science and Engineering Foundation. A.E.E. acknowledges support from the Miller Institute for Basic Research in Science at the University of California, Berkeley, from NSF ITR ACI-0121671 and from NASA ATP NAG5-13378.

REFERENCES

Agustsson, I., & Brainerd, T. G. 2006, ApJ, 644, L25

Atlay, G., Colberg, J. M., Croft, R. A. C. 2006, MNRASin press, preprint [astro-ph/0605296]

Bardeen, J.M., Bond, J. R., Kaiser, N., Szalay, A.S. 1986, apj, 304, 15

Basilakos, S. 2006, MNRAS, 344, 602

Basilakos, S., Plionis, M. et al. 2006, MNRAS, 365, 539

Bond, J., R., Kofman, L., & Pogosyan, D. 1996, Nature, 380, 603

Brainerd, T. G. 2005, ApJ, 628, L101

Busha, M.T., Evrard, A.E., Adams, F.C.& Wechsler, R.H. 2005, MNRAS, 363, 11

Dubinski, J. 1998, ApJ, 502, 141

Eke, V., Cole, S., & Frenk, C. 1996, MNRAS, 283, 263

Evrard, A. E, et al. 2002, ApJ, 573, 7

Faltenbacher, A., Kerscher, A., Gottloeber, S., & Mueller, M. 2002, A&A, 395, 1

Fuller, T. M., West, M. J., & Bridges, T. J. 1999, ApJ, 519, 22,

Kalinkov, M., Valtchanov, I., & Kuneva, I. 1998, ApJ, 506, 509

Kang, X., Mao, S., Gao, L., & Jing, Y. P. 2005, A&A, 437, 383

Kasun, S. F., & Evrard, A. E. 2005, ApJ, 629, 781

Knebe, A. et al. 2004, ApJ, 603, 7

Kroupa, P., Theis, C., & Boily, C. M. 2005, A&A, 431, 517

Lee, J. & Pen, U. L. 2000, ApJ, 532, L5

Lee, J. & Pen, U. L. 2001, ApJ, 555, 106

Lee, J., Kang, X., & Jing, Y. 2005, ApJ, 629, L5

Lee, J. & Kang, X. 2006, ApJ, 637, 561

Libeskind, N. I., Frenk, C. S., Cole, S., Helly, J. C., Jenkins, A., Navarro, J. F., & Power, C. 2005, preprint (astro-ph/0503400)

MacGillivray, H. T., Dodd, R. J., McNally, B. V., & Corwin, H. G. 1982, MNRAS, 198, 605

Macfarland, T., Couchman, H. M. P., Pearce, F. R., & Pichlmeier, J. 1998, NewA, 3, 687

Nagamine, K., & Loeb, A. 2003, NewA, 8, 439

Onuora, L. I., & Thomas, P. A. 2000, MNRAS, 319, 614

Pereira, M. J., & Kuhn, J. R. 2005, 627, L21

Plionis, M. 1994, ApJS, 95, 401

Plionis, M. 2002, in Modern Theoretical and Observational Cosmology, (Kluwer Academic Publishers: Dordrecht), p.299

Plionis, M., & Basilakos, S. 2002, MNRAS, 329, L47

Plionis, M., Benoist, C., et al. 2003, ApJ, 594, 153

Plionis, M. 2004, Ourskirts of Galaxy Clusters, (Cambridge Univ. Press: Cambridge), p. 19 (Kluwer Academic Publishers: Dordrecht), p.299

Pogosyan, D., Bond, J. R., Kofman, L., & Wadsley, J. 1998, Wide Field Surveys in Cosmology, (Frontiers: Paris), p. 61

Shapley, H. 1930, Harvard Obs. Bull., 874, 9

Springel, V., White, S. D. M., Tormen, G., Kauffmann, G. 2001, MNRAS, 328, 726

Valtonen, M., Teerikorpi, P., & Argue, A. 1978, AJ, 83, 135

van Haarlen, M., & van de Weygaert, R. 1993, ApJ, 418, 544

West, M. J. 1989, ApJ, 347, 610

West, M. J., Willumsen, C., & Dekel, A. 1991, ApJ, 369, 287

Zel'dovich, Y. B. 1970, A& A, 5, 84

Zentner, A. R., Kravtsov, A. V., Gnedin, O. Y., & Klypin, A. A. 2005, 629, 219

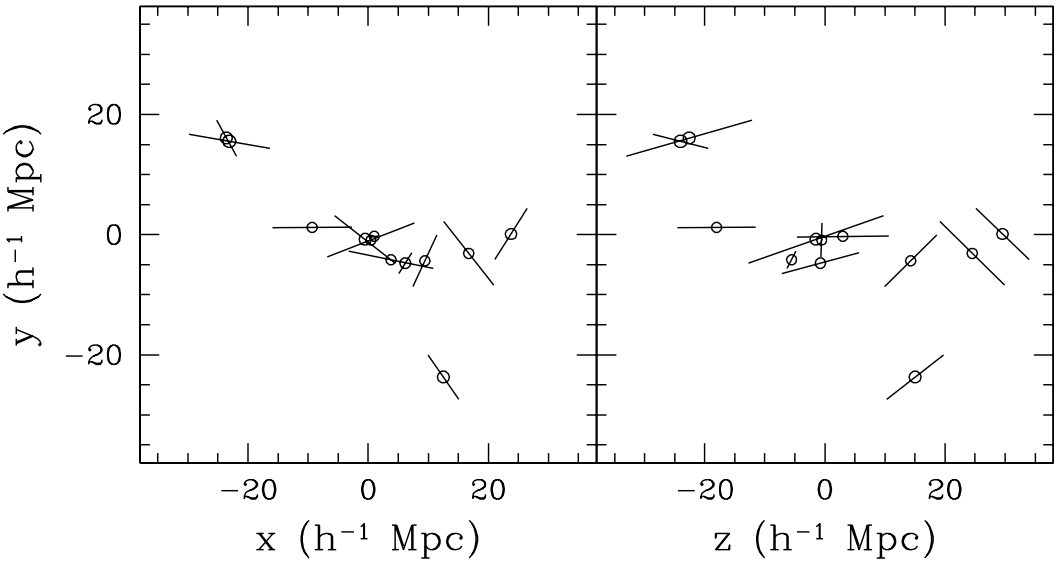

Fig. 1.— The spatial distribution of the third richest supercluster is shown in orthogonal projections. Circles show halo locations, with symbol size scaling as $M^{1/3}$, while lines through each halo show the orientation of the major axis of its density field, taken from (Kasun & Evrard 2005). The length of each line is proportional to the halo's major-to-minor axis ratio.

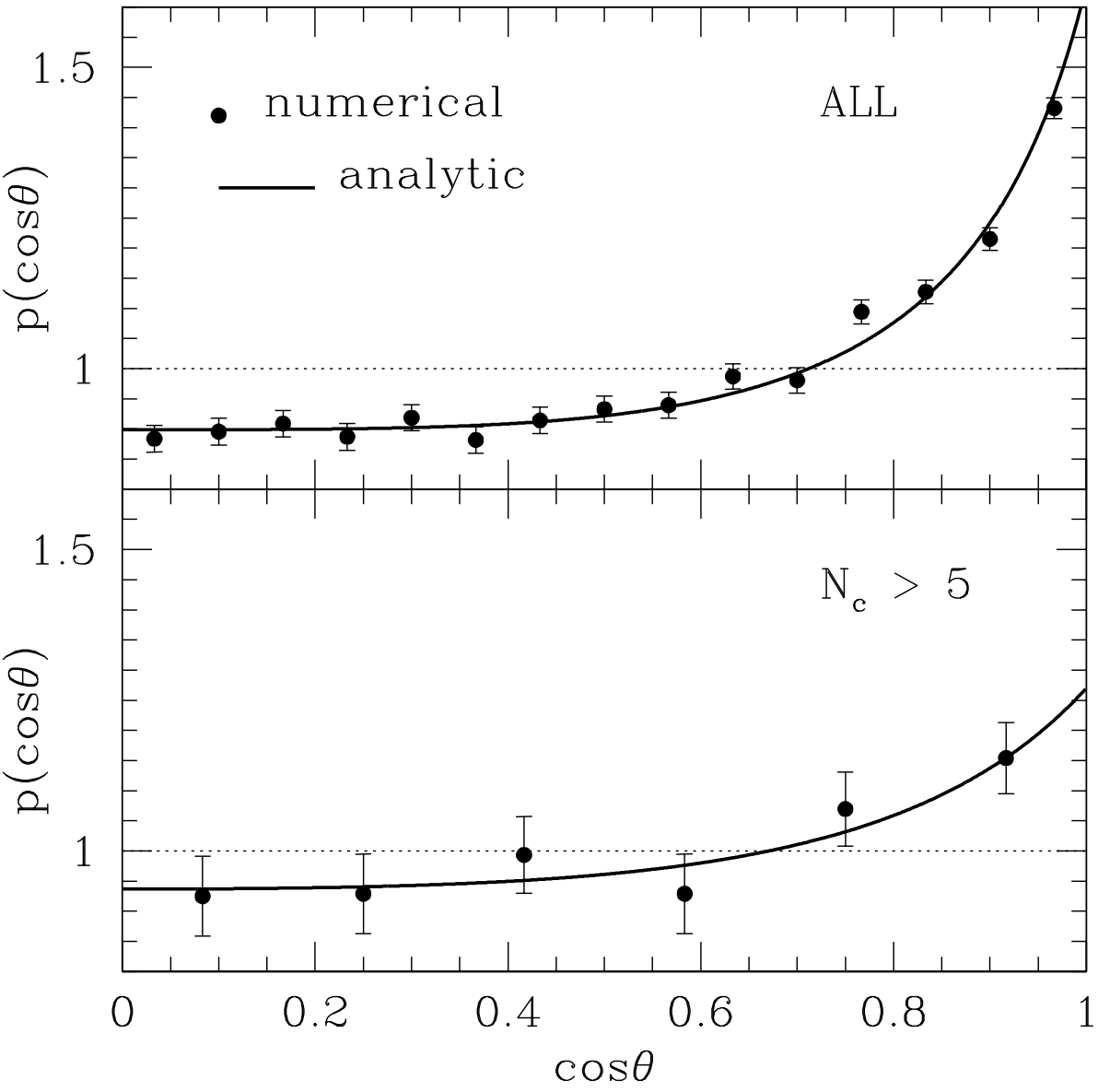

Fig. 2.— Probability density distributions of the cosines of the angles between the major axes of clusters and their superclusters: (*Upper*): the case that all 14007 superclusters are used; (*Lower*): the case that only 217 superclusters with more than five clusters are used. In each panel, the numerical result is represented by dots with Poissonian errors while the analytic result (5) corresponds to the solid curve. The dotted line corresponds to the case of no alignment.

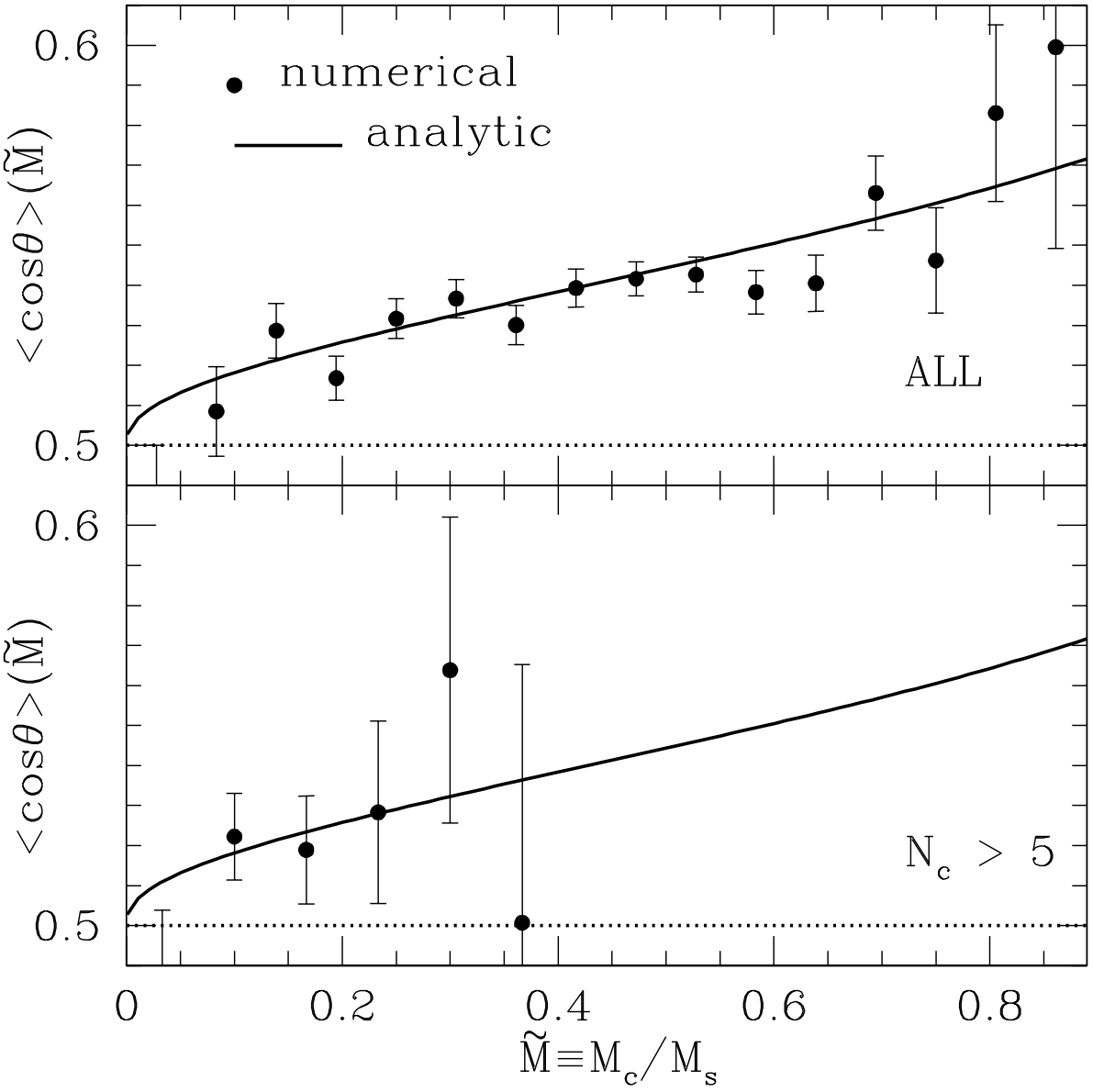

Fig. 3.— Average of the cosines of the angles as a function of the cluster mass: (*Upper*): the case that all 14007 superclusters are used; (*Lower*): the case that only 217 superclusters with more than five clusters are used. In each panel, the dots and solid curves represent the numerical and the analytic results, respectively. The errors are calculated as one standard deviation of the cosines of the angles for the case of no alignment. The dotted line corresponds to the case of no alignment.

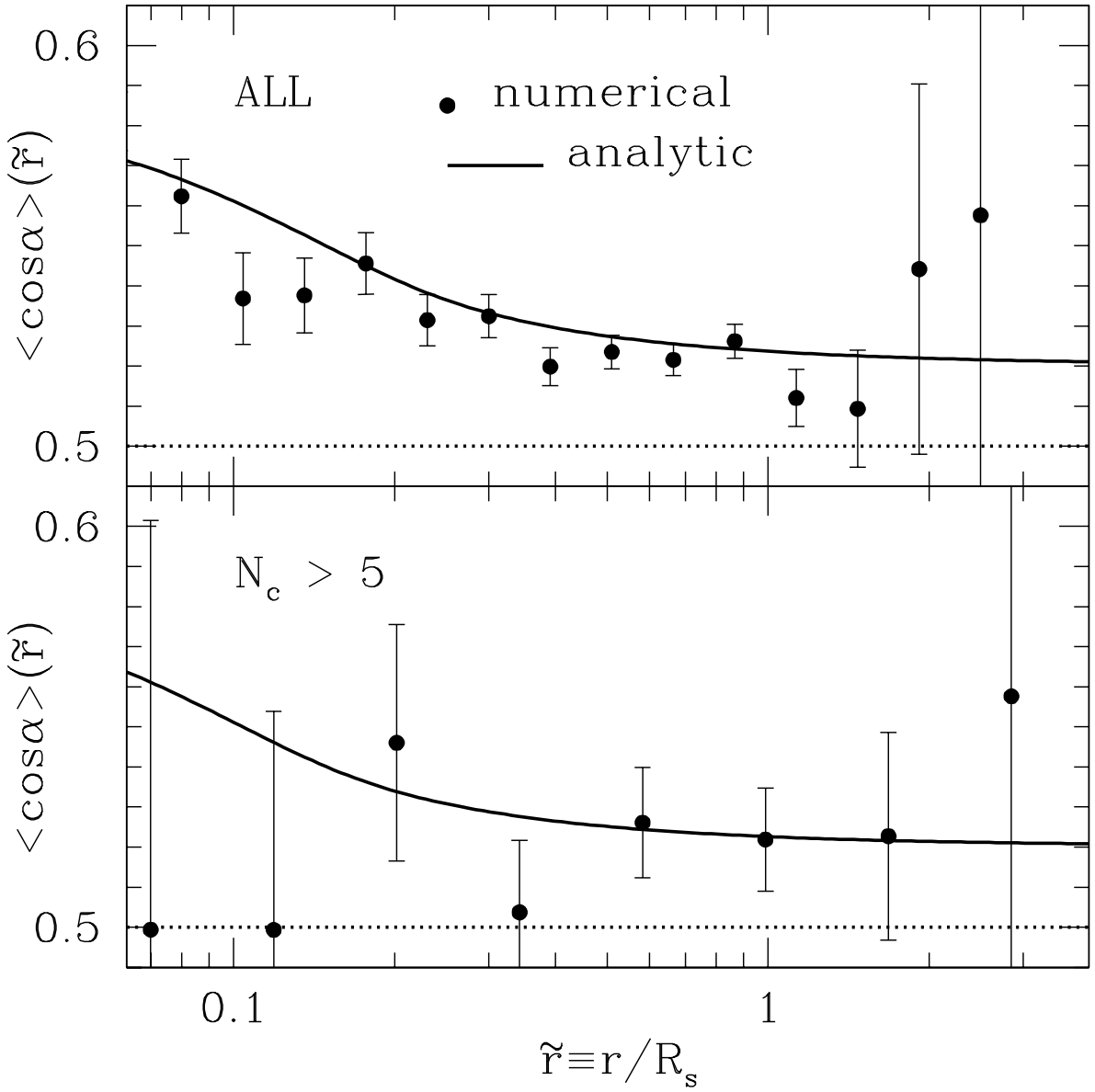

Fig. 4.— Average of the cosines of the angles as a function of the distance from the supercluster center to the cluster center: (*Upper*): the case that all 14007 superclusters are used; (*Lower*): the case that only 217 superclusters with more than five clusters are used. In each panel the dots and solid curves represent the numerical and the analytic results, respectively. The dotted line corresponds to the case of no alignment.

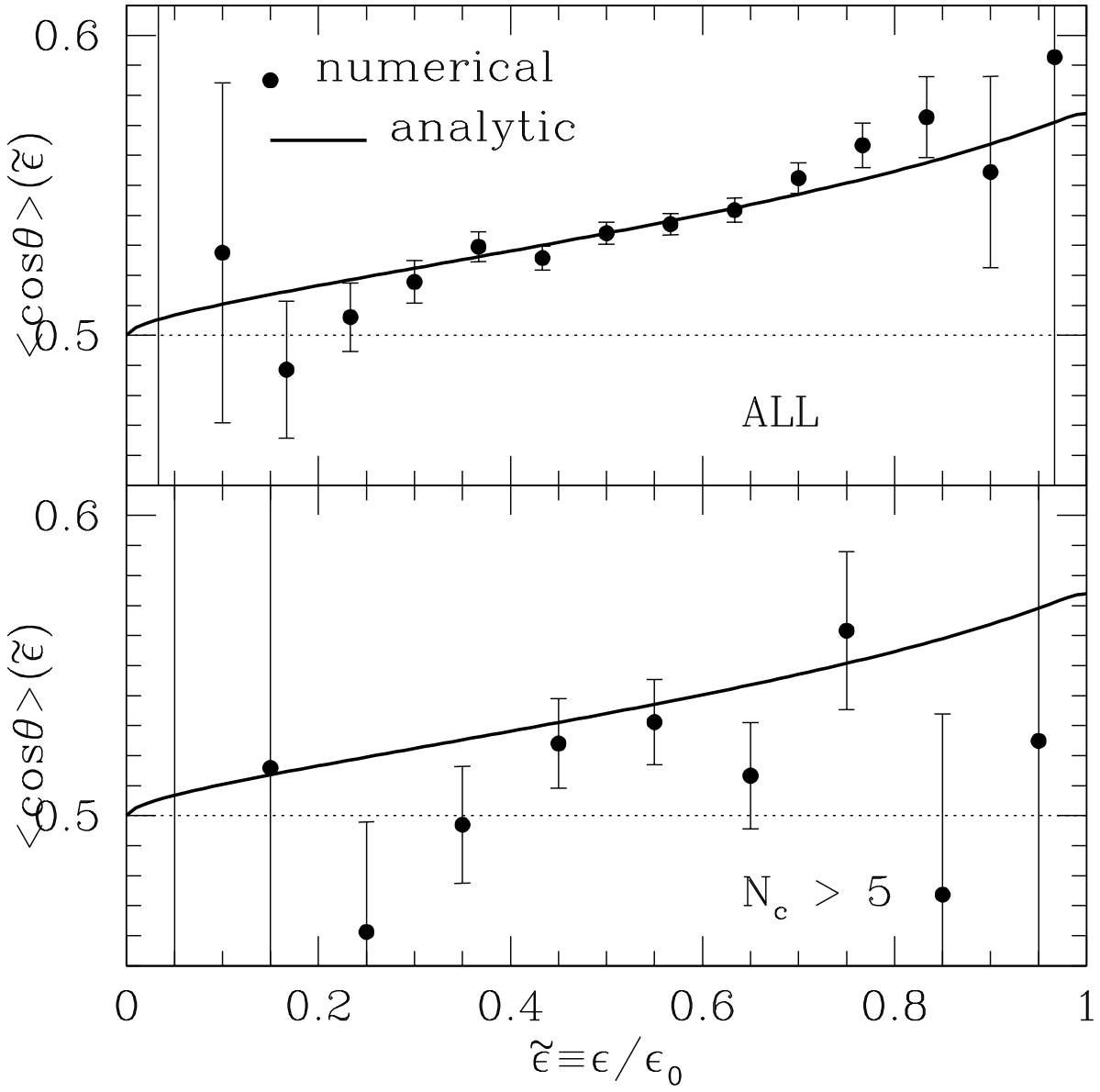

Fig. 5.— Average of the cosines of the angles as a function of the cluster ellipticity: (*Upper*): the case that all 14007 superclusters are used; (*Lower*): the case that only 217 superclusters with more than five clusters are used. In each panel, the dots and solid curves represent the numerical and the analytic results, respectively. The dotted line corresponds to the case of no alignment.

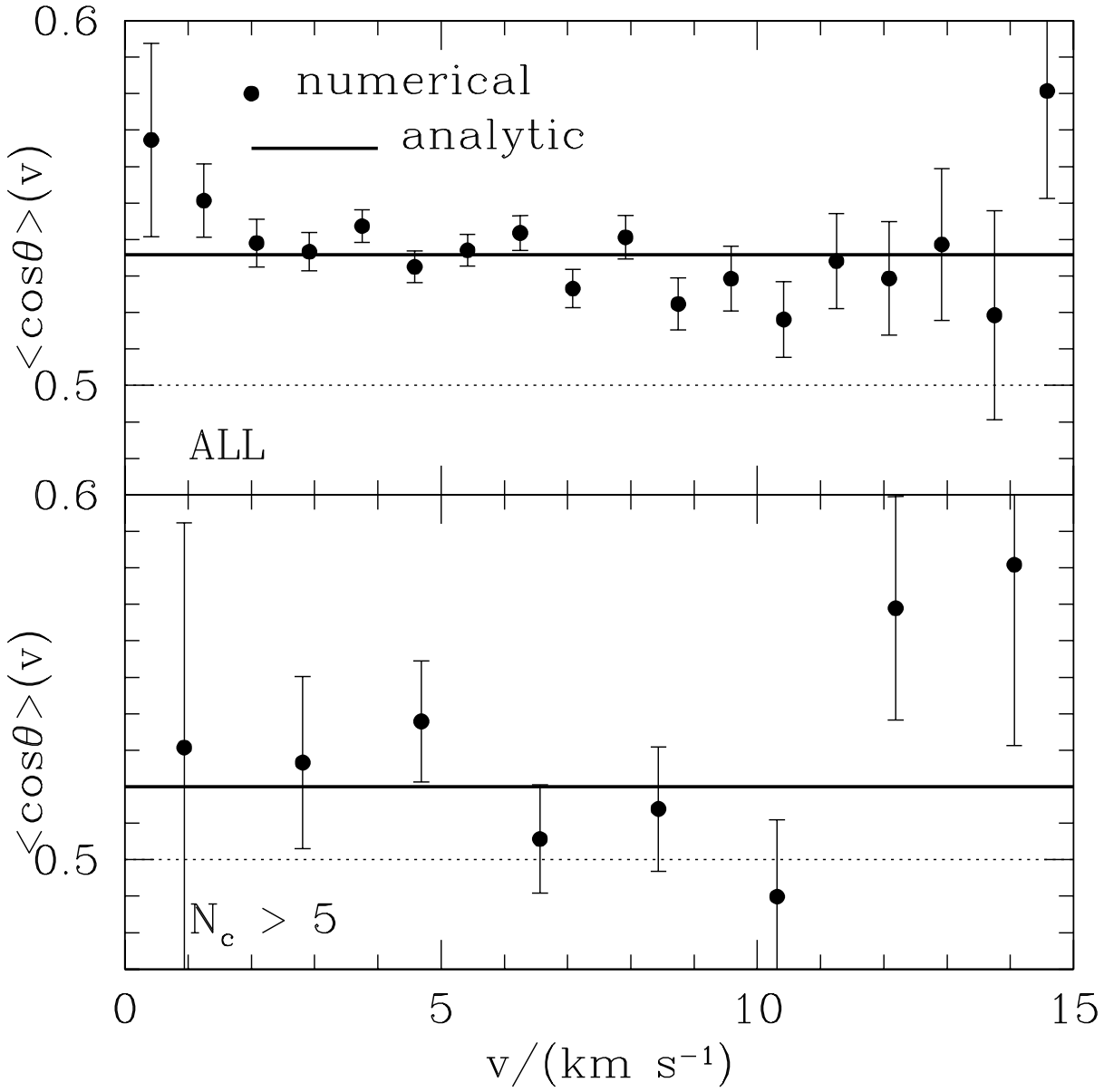

Fig. 6.— Average of the cosines of the angles as a function of the cluster velocity: (*Upper*): the case that all 14007 superclusters are used; (*Lower*): the case that only 217 superclusters with more than five clusters are used. In each panel, the dots and solid curves represent the numerical and the analytic results, respectively. The dotted line corresponds to the case of no alignment.